Current-induced enhancement of photo-response in graphene THz radiation detectors

K. Indykiewicz, Cédric Bray, C. Consejo, F Teppe, S. Danilov, S. Ganichev, A. Yurgens

Current-induced enhancement of photo-response in graphene THz radiation detectors

Cite as: AIP Advances 12, 115009 (2022); doi: 10.1063/5.0117818
Submitted: 28 August 2022 • Accepted: 10 October 2022 •
Published Online: 4 November 2022

K. Indykiewicz,[1,5] C. Bray,[2] C. Consejo,[2] F. Teppe,[2] S. Danilov,[3] S. D. Ganichev,[3,4] and A. Yurgens[5,a)]

AFFILIATIONS

[1] Faculty of Electronics, Photonics and Microsystems, Wrocław University of Science and Technology, 50-372 Wrocław, Poland
[2] CNRS/Laboratoire Charles Coulomb (L2C), 34095 Montpellier, France
[3] University of Regensburg, Faculty of Physics, D-93053 Regensburg, Germany
[4] CENTERA Laboratories, Institute of High Pressure Physics, Polish Academy of Sciences, PL-01-142 Warsaw, Poland
[5] Chalmers University of Technology, MC2, SE-412 96 Göteborg, Sweden

[a)] **Author to whom correspondence should be addressed:** yurgens@chalmers.se

ABSTRACT

Thermoelectric readout in a graphene terahertz (THz) radiation detector requires a *p-n* junction across the graphene channel. Even without an intentional *p-n* junction, two latent junctions can exist in the vicinity of the electrodes/antennas through the proximity to the metal. In a symmetrical structure, these junctions are connected back-to-back and therefore counterbalance each other with regard to rectification of the ac signal. Because of the Peltier effect, a small dc current results in additional heating in one and cooling in another *p-n* junction, thereby breaking the symmetry. The *p-n* junctions then no longer cancel, resulting in a greatly enhanced rectified signal. This allows simplifying the design and controlling the sensitivity of THz radiation detectors.

Graphene-based terahertz (THz) detectors can be fast and sensitive devices in a wide frequency range.[1,2] There are several readout mechanisms in graphene detectors, such as bolometric,[3] thermoelectric (TEP),[4] and ballistic readout mechanisms[5] and those based on noise thermometry,[6] ratchet effects,[7,8] and electron-plasma waves,[9,10] also called the Dyakonov–Shur (D–S) mechanism.[11,12] Detectors with the TEP readout mechanism are simple, do not require electrical bias, and therefore have no $1/f$ noise, allowing for scalable fabrication using chemically vapor-deposited (CVD) graphene, and have undemanding electrical contacts. The high efficiency of such detectors stems from a large radiation-induced increase in the electronic temperature T_e because of the weak electron–phonon (*e-ph*) coupling in graphene[13,14] and a large value of the Seebeck coefficient ($S \sim T_e/3\ \mu$V/K).[15,16]

A *p-n* junction across the graphene channel must be formed to fully realize the TEP readout in a graphene-based radiation detector [see Fig. 1(a)]. It can be done either chemically or electrostatically by using a split top gate.[17] Without *p-n* junctions, the TEP signal is usually insignificant.[1,2]

However, there can be latent *p-n* (or *p-p′* or *n-n′*) junctions in the vicinity of the electrodes/antennas through the proximity to the metal.[19–21] These junctions do not normally contribute to rectification[22] of the ac current induced by THz radiation because the junctions (diodes) are connected back to back, i.e., symmetrically in the opposite directions [see Fig. 1(b)]. Here, we show experimentally and by numerical simulations that a small dc current breaks the symmetry and the ac current gets rectified, which considerably increases the signal. This allows for effective control of sensitivity of the THz-radiation detector.

We fabricated the devices from a chemically vapor-deposited (CVD) graphene grown on a 2 in. large copper foil 25- or 60-μm thick in a commercial cold-wall CVD system (AIXTRON Black Magic II). Pure Ar and H_2 were used as a buffer- and nucleation-controlling gas, respectively. The precursor gas was CH_4 diluted in Ar (5%). The nominal temperature was regulated by using a thermocouple in contact with the graphitic heater. Many patches of two- and three-layer graphene were seen in the majority of samples. The resulting charge-carrier mobility μ

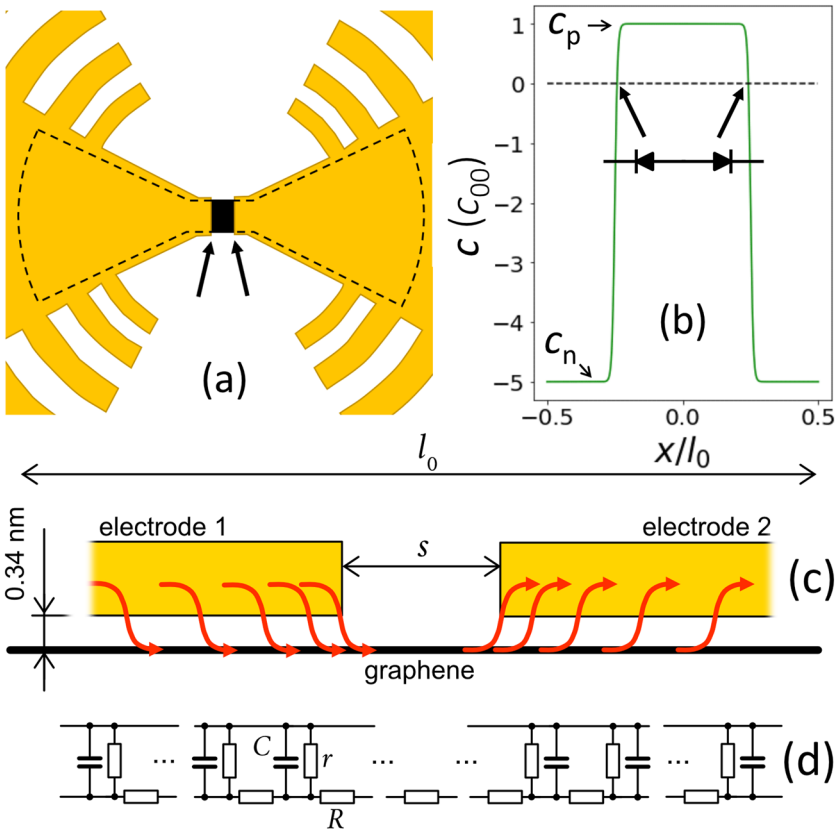

FIG. 1. (a) Model geometry of a symmetric graphene detector. Graphene is outlined by the dashed line. The arrows mark two latent *p-n* junctions in the vicinity of the electrodes (log-periodic antenna in this case). (b) Schematic doping profile in a device. The regions under the electrodes are assumed to be *n* doped because of the proximity to the metal. The latent *p-n* junctions (diodes) are connected back to back (the inset). (c) Schematic cross section of the graphene channel with two metal electrodes. Red arrows show a current flow and its distribution (crowding). (d) Lumped-element representation of the device, where C, R, and $G = 1/r$ are the capacitance, graphene resistance, and contact conductance per unit length, respectively. Note the similarity with the classical transmission line (see, e.g., Ref. 18 or refer to Wikipedia), allowing for straightforward estimation of the current-crowding length $\lambda_j = 1/\sqrt{RG} \sim 1 - 5\ \mu$m. In the self-gating scenario, R is a function of the local voltage drop V_l across the contact resistance r, $R = \mu^{-1}(C^2V_l^2 + c_{00}^2e_0^2)^{-0.5}$, which introduces significant non-linearity at high bias. Here, c_{00} is the residual charge density, and e_0 is the electron charge.

of such graphene transferred to ordinary office lamination foil [ethylene vinyl acetate(EVA)/polyethylene terephthalate (PET)] was nonetheless surprisingly high, reaching 9000 $cm^2/(Vs)$.[23,24]

THz detectors were fabricated in many ways, with graphene both under and on top of the metal electrodes/antennas. We also chose different metals for the electrodes—Au, Pt, and Pd—which were expected to have different proximity-doping effects on graphene.[19] CVD graphene was either transferred to a SiO_2/Si substrate by using the PMMA- or paraffin-assisted technique[25] or simply glued to a substrate using an epoxy-based adhesive. Bow-tie or log-periodic antennas were lithographically patterned to have better coupling to THz radiation [see Fig. 1(a)]. However, the antennas appeared to only play a minor role in the frequency range of our measurements because of a relatively high graphene-to-metal contact resistance, resulting in a significant impedance mismatch. This leaves spacey room for uncomplicated improvement of detectors in the future, promising a much better performance than that demonstrated in this work.

For optical excitation, we used Gunn diodes and pulsed THz laser[26,27] optically pumped by a transversely excited atmospheric-pressure CO_2 laser.[28] The Gunn diode provided linearly polarized radiation with a frequency of 94 GHz and an estimated incident power of 1–10 mW. The radiation was modulated using an optical chopper at a frequency of 37 Hz, allowing measurements of photoresponse using the standard lock-in technique. The THz power delivered to the samples in the cryostat through the optical windows is somewhat difficult to reliably estimate because of the multiple reflections from the metal walls of the cryostat, resulting in light interference and a complex pattern of maxima and minima of the light intensity.

The THz laser provides single pulses of monochromatic radiation, with the pulse duration in the order of 100 ns, a repetition rate of 1 Hz, and the peak power in the order of hundreds of kW. The peak power was monitored using THz photon-drag detectors.[29] The laser operated at frequencies $f = 0.61$, 1.07, 2.02, and 3.31 THz. The photoresponse to the THz pulses was measured using a digital oscilloscope as a voltage drop across a 50 Ω load resistor.

Figure 2(a) shows the response signal vs dc current, demonstrating an initially linear increase in the signal and then a tendency to saturate and even decrease at the maximum current. The sign of the signal changes with the direction of the dc current. In the samples with dissimilar metals on both ends of the graphene channel, there was usually an offset in the vertical direction common to all curves, which meant that the signal at low temperature was significant even at zero dc current.

The signal decreases with temperature [see Fig. 2(b)]; the shape of this decreasing function is sample dependent. As shown in Fig. 2(b), the signal changes gradually and survives up to room temperature. However, in several other samples, the signal decayed to zero at 150–200 K. A couple of devices showed a very abrupt change in the signal that vanished at ~40 K (see the supplementary material).

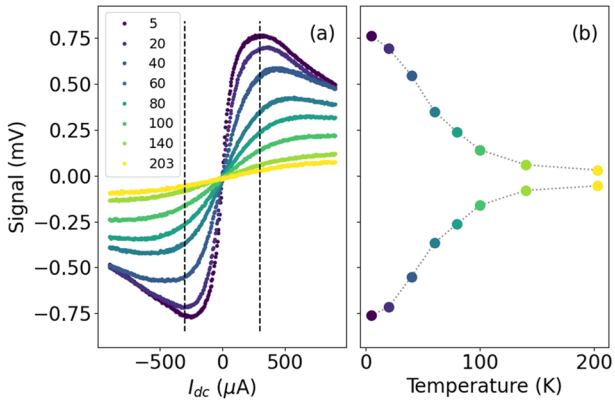

FIG. 2. (a) Output response signal to 94 GHz radiation vs dc current and (b) the temperature dependence of the signal at the two fixed dc currents marked by the vertical dashed lines.

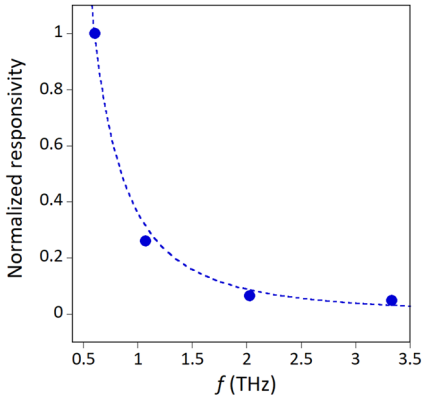

FIG. 3. Normalized responsivity $\hat{r}$ for the linear-polarized THz pulsed radiation at T_0 = 300 K. The normalization constant is 0.072 μV/W. The dotted line is a fit to the equation $\hat{r} = (f_0/f)^2$, with the parameter $f_0 \approx 0.6$ THz.

The mechanism behind this temperature dependence is unclear and requires further experiments.

Since the response signal in our devices is due to the thermoelectric effects and involves electron heating, the decay of the signal with temperature should be largely attributed to the increased cooling of hot electrons. The electrons are cooled by interactions with phonons. These interactions are generally weak because the population of optical phonons is exponentially small at low temperature. The cooling efficiency through the acoustical phonons is impeded because of the momentum mismatch but can be somewhat improved when involving scattering by impurities (supercollisions).[13] However, there can be many other modes involving the out-of-plane direction in multilayer graphene, e.g., the shear mode at 31 cm^{-1}.[30,31] Many double-layer patches and these phonons can, in principle, be an effective channel for cooling the electrons.

The heating of electrons can be regarded by simply considering graphene as a conducting layer with Drude-like frequency-dependent conductivity $\sigma(\omega) = \sigma_0(1 - i\omega\tau)^{-1}$. The heating effects are described by the real part of the conductivity, $P(\omega) \sim v^2\,\mathrm{Re}(\sigma(\omega)) \sim v^2\sigma_0/(\omega\tau)^2$, for $\omega\tau \geq 1$. Here, P is the Joule heating power, v is the ac-voltage amplitude in graphene, σ_0 is the dc conductivity, τ is the scattering time, $\omega = 2\pi f$, and f is the frequency.

Figure 3 shows the frequency dependence of the normalized response signal at room temperature. By rotating the electric field vector with respect to the line connecting the contacts, we observed only weak polarization dependence of the photoresponse, which confirms the anticipated inefficiency of the antennas because of the large impedance mismatch. The overall responsivity decays with the frequency as $1/f^2$ (see the dashed line in Fig. 3), in correspondence with the suggested Drude model for Joule heating by THz radiation.[32]

When applying perpendicular magnetic field to graphene, we observed that the photoresponse substantially decreased. This is shown in Fig. 4. Overall, the decrease in the signal in the magnetic field can be explained by the increased relaxation of electrons, causing a decrease in their temperature and thermoelectric response. Indeed, it was experimentally observed in graphene with defects that the relaxation of hot electrons would increase in the perpendicular magnetic field. This was attributed to the supercollision cooling combined with the presence of mirror-plane-symmetry-breaking defects in graphene.[33] It was suggested that the defect–electron interaction could activate the out-of-plane phonons at the Γ point (ΓZO phonons). Supercollisions involving these phonons would then allow transitions between the sufficiently broadened lowest Landau levels in realistic magnetic fields, thereby opening an additional channel for electron-energy relaxation.[33]

Many double-layer patches in our graphene devices could be symmetry-breaking defects, validating this scenario. Moreover, the presence of soft shear-mode phonons (31 cm^{-1}) in multi-layer graphene can further emphasize the supercollision cooling in the magnetic field.[30] The shear mode energy roughly corresponds to 40 K when the population of these phonons is expected to dramatically increase and provide an additional pathway for electron energy relaxation. This might be the reason for the sudden

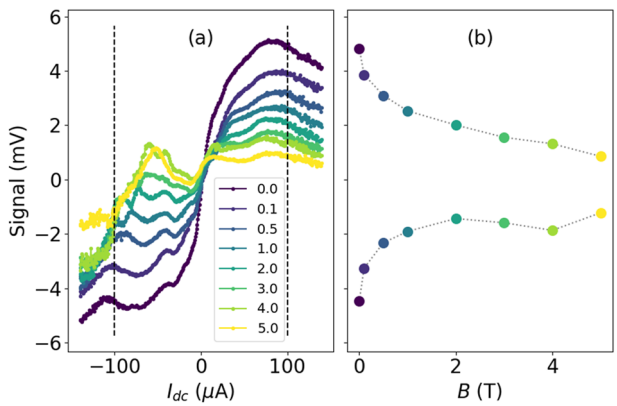

FIG. 4. (a) Response signal as a function of the dc current in different magnetic fields at 1.7 K. Note the overall decrease in the signal as the magnetic field increases. (b) The signal vs the magnetic field B at two dc currents, indicated by the vertical dashed lines in (a).

disappearance of the signal at this temperature in a couple of our samples (see Fig. S2).

Some wiggles are also seen in the curves at 1.7 K (see Fig. 4). They are visible even at zero field but not in all samples (see, e.g., Fig. 2) and become more pronounced with an increasing magnetic field. The structures are clearly seen only at negative dc currents. The nature behind these structures is not known and requires further studies. Possible explanations include plasma resonances[9] or some microwave interference effects in the cavity formed between the metallic sample holder and the electrodes, with graphene and the dielectric substrate in between. The self-doping effect under the electrode can, in principle, explain the asymmetry with regard to the current direction in the latter case.

The ac response resulting from the dc bias in completely symmetric graphene-metal structures can be explained in two ways. One assumes the self-gating effect in the top contacts to graphene. Another takes into account the non-uniform doping in graphene because of proximity to metals. It can also be a combination of the two mechanisms in real devices. Both mechanisms are similar, in which Joule heating and thermoelectric effects give rise to a rectified signal because of spatially non-uniform doping in graphene. The difference is in the manner of how the non-uniformity is created—through self-gating or proximity doping (see Fig. 1). Here, we outline a general model of thermal balance between electron and phonon subsystems in graphene that is subject to Joule heating, in the presence of thermoelectric effects and non-uniform doping.

A graphene strip of length l_0 and width w is subdivided into p- and n-regions [see Fig. 1(b)]. The p region corresponds to the graphene channel in between the source and drain contacts, while n regions correspond to graphene under the contacts because of proximity doping in graphene.[34]

The strip rests on a 300 nm thick SiO_2 layer on top of the Si substrate at constant temperature T_0. The electrical current with linear density j flows in the x direction from the source-to-drain electrodes. Electrons in graphene are heated by the current and cooled by phonons through the electron–phonon interaction. Phonons escape into the Si substrate via thermal resistance of the SiO_2 layer, which results in an increased lattice temperature $T_{ph} > T_0$. The heating and the temperature distribution $T_e(x)$ are highly non-uniform because the spatially varying doping profile $c(x)$ results in non-uniform conductance and, hence, Joule heating. Moreover, it gives rise to a non-uniform Seebeck coefficient $S = S(x)$ and the Peltier effect $(jT_e\partial S/\partial x)$. This model is described by the coupled one-dimensional heat-diffusion equations,

$$-\frac{\partial}{\partial x}\left(\kappa_e\frac{\partial T_e}{\partial x}\right) = \frac{j^2}{\sigma} - jT_e\frac{\partial S}{\partial x} - \alpha_i\left(T_e^i - T_{ph}^i\right), \quad (1)$$

$$-\kappa_{ph}\frac{\partial^2 T_{ph}}{\partial x^2} = \alpha_i\left(T_e^i - T_{ph}^i\right) - \kappa_0\left(T_{ph} - T_0\right), \quad (2)$$

where $\kappa_e = L_0\sigma T$ is the electronic sheet thermal conductivity; L_0 is the Wiedemann–Franz constant; T_e, T_{ph}, k_e, and k_{ph} are the temperatures and thermal conductivities of electronic (e) and phononic (ph) subsystems, respectively; and κ_0 is the thermal conductivity of the 300 nm thick SiO_2 layer. The Seebeck coefficient S in graphene is assumed to obey Mott's equation. The heat transfer to the phonon system is described by the last term in Eq. (1). The exponent $i = 3$ or $i = 4$ at temperatures above or below the Bloch-Grüneisen temperature T_{BG}, respectively, and $\alpha_3 \propto c$.[13]

Numerically solving Eqs. (1) and (2) gives $T_e(x)$, $T_{ph}(x)$, the TEP voltage, and the total Joule dissipation for any bias current j. The current in real detectors will be a sum of the dc- and ac components: $j(t) = j_{dc} + j_0\sin(\omega t)$. For $\omega \ll 2\pi/\tau$, where $\tau < 50$ fs is the electron-heating time,[35] the responsivity can be found by averaging the TEP voltage and Joule power over one period of the ac bias. The simulation details can be found in the supplementary material and Ref. 36.

Simulations were conducted for various sets of parameters, giving somewhat different shapes of the resulting curves, depending on the parameters. In Fig. 5, it is seen, e.g., that the signal can even change sign as a function of dc current. The phenomenological fit shown in Fig. 5(b) has no real significance even though it reveals a T^{-3} factor, which much likely stems from the cooling term in Eq. (1).

The main parameters that affect the shape of the curves are doping and residual charge densities. The signal amplitude is at maximum when there are p-n junctions at the edges of the electrodes. In the case of n-n' or p-p' junctions, the signal is reduced. This is understandable from the fact that the graphene sheet resistance (and, hence, Joule heating) is at maximum where the doping is zero. The current crowding is beneficial because it also results in the Joule heating that takes place largely at the electrode edges. The maximum temperature increase in the p-n junctions leads to the large thermoelectric voltage and an increased signal as well.

In summary, we have shown that in symmetric graphene radiation detectors, the symmetry can be lifted by application of dc current. This leads to a non-compensated response of the detectors because of nonequivalent thermal conditions for the two p-n junctions at the edges of the metal electrodes. One p-n junction is biased in the forward direction while another is biased in the reverse direction, corresponding to Peltier heating and cooling, respectively. The p-n junctions can be formed because of the proximity

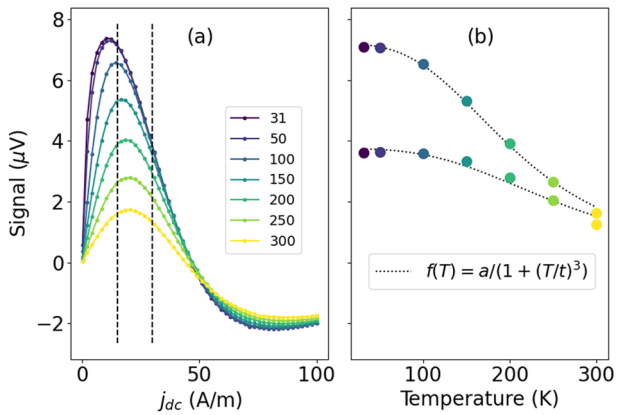

FIG. 5. (a) Simulated response signal vs dc current at different temperatures. The following parameters were used: c_{00}, c_p, and c_n = 0.5, 1, and -5×10^{12} cm^{-2}, λ_j = 1 μm, and j_{ac} = 1 A/m [see also Fig. 1(b)]. (b) The temperature dependence of the maximum signal and the best fit to the empirical equation $f(T) = a/[1 + (T/t)^3]$, with t = 210 and 264 K for the top and bottom curve, respectively.

doping or self-gating effect under the metal electrodes. The simulations reveal several possible scenarios of the current-induced response to THz radiation, depending on the metals used and residual doping of graphene. The thermoelectric effect is at the center of all the observations. All in all, our work paves the way for design of graphene radiation detectors with controllable responsivity.

SUPPLEMENTARY MATERIAL

See the supplementary material for details of the samples' fabrication, their characterization, and the results of simulations.

ACKNOWLEDGMENTS

This work was supported by the FLAG-ERA Program (Project DeMeGRaS, VR2019-00404, DFG No. GA 501/16-1, and ANR-19-GRF1-0006), the Terahertz Occitanie Platform, and by the CNRS through IRP "TeraMIR." F.T. and S.D.G. thank the support from the IRAP Program of the Foundation for Polish Science (Grant No. MAB/2018/9, Project CENTERA). This work was performed in part at Myfab Chalmers.

AUTHOR DECLARATIONS

Conflict of Interest

The authors have no conflicts to disclose.

Author Contributions

K. Indykiewicz: Data curation (supporting); Investigation (equal); Methodology (equal); Visualization (supporting). **C. Bray**: Data curation (equal); Formal analysis (equal); Visualization (equal). **C. Consejo**: Data curation (equal); Formal analysis (equal); Methodology (equal). **F. Teppe**: Conceptualization (equal); Data curation (supporting); Formal analysis (equal); Supervision (equal); Writing – review & editing (supporting). **S. Danilov**: Data curation (equal); Formal analysis (equal); Visualization (equal). **S. D. Ganichev**: Conceptualization (equal); Data curation (supporting); Formal analysis (supporting); Investigation (supporting); Methodology (supporting); Supervision (equal); Writing – review & editing (equal). **A. Yurgens**: Conceptualization (lead); Formal analysis (lead); Funding acquisition (equal); Investigation (equal); Methodology (equal); Project administration (lead); Software (lead); Supervision (equal); Validation (equal); Visualization (equal); Writing – original draft (lead); Writing – review & editing (lead).

DATA AVAILABILITY

The data that support the findings of this study are available from the corresponding author upon reasonable request.

REFERENCES

[1] L. Vicarelli, M. S. Vitiello, D. Coquillat, A. Lombardo, A. C. Ferrari, W. Knap, M. Polini, V. Pellegrini, and A. Tredicucci, "Graphene field-effect transistors as room-temperature terahertz detectors," Nat. Mater. **11**, 865 (2012).

[2] F. H. L. Koppens, T. Mueller, P. Avouris, A. C. Ferrari, M. S. Vitiello, and M. Polini, "Photodetectors based on graphene, other two-dimensional materials and hybrid systems," Nat. Nanotechnol. **9**, 780 (2014).

[3] A. El Fatimy, R. L. Myers-Ward, A. K. Boyd, K. M. Daniels, D. K. Gaskill, and P. Barbara, "Epitaxial graphene quantum dots for high-performance terahertz bolometers," Nat. Nanotechnol. **11**, 335–338 (2016).

[4] X. Cai, A. B. Sushkov, R. J. Suess, M. M. Jadidi, G. S. Jenkins, L. O. Nyakiti, R. L. Myers-Ward, S. Li, J. Yan, D. K. Gaskill, T. E. Murphy, H. D. Drew, and M. S. Fuhrer, "Sensitive room-temperature terahertz detection via the photothermoelectric effect in graphene," Nat. Nanotech. **9**, 814 (2014).

[5] G. Auton, D. B. But, J. Zhang, E. Hill, D. Coquillat, C. Consejo, P. Nouvel, W. Knap, L. Varani, F. Teppe, J. Torres, and A. Song, "Terahertz detection and imaging using graphene ballistic rectifiers," Nano Lett. **17**, 7015–7020 (2017).

[6] K. C. Fong and K. C. Schwab, "Ultrasensitive and wide-bandwidth thermal measurements of graphene at low temperatures," Phys. Rev. X **2**, 031006 (2012).

[7] P. Olbrich, J. Kamann, M. König, J. Munzert, L. Tutsch, J. Eroms, D. Weiss, M.-H. Liu, L. E. Golub, E. L. Ivchenko, V. V. Popov, D. V. Fateev, K. V. Mashinsky, F. Fromm, T. Seyller, and S. D. Ganichev, "Terahertz ratchet effects in graphene with a lateral superlattice," Phys. Rev. B **93**, 075422 (2016).

[8] D. V. Fateev, K. V. Mashinsky, and V. V. Popov, "Terahertz plasmonic rectification in a spatially periodic graphene," Appl. Phys. Lett. **110**, 061106 (2017).

[9] D. A. Bandurin, D. Svintsov, I. Gayduchenko, S. G. Xu, A. Principi, M. Moskotin, I. Tretyakov, D. Yagodkin, S. Zhukov, T. Taniguchi, K. Watanabe, I. V. Grigorieva, M. Polini, G. N. Goltsman, A. K. Geim, and G. Fedorov, "Resonant terahertz detection using graphene plasmons," Nat. Commun. **9**(1–8), 5392 (2018).

[10] A. Tomadin and M. Polini, "Theory of the effective Seebeck coefficient for photoexcited two-dimensional materials: Graphene," Phys. Rev. B **104**, 125443 (2021).

[11] M. Dyakonov and M. Shur, "Detection, mixing, and frequency multiplication of terahertz radiation by two-dimensional electronic fluid," IEEE Trans. Electron. Dev. **43**, 380–387 (1996).

[12] M. Dyakonov and M. Shur, "Shallow water analogy for a ballistic field effect transistor: New mechanism of plasma wave generation by dc current," Phys. Rev. Lett. **71**, 2465–2468 (1993).

[13] A. C. Betz, S. H. Jhang, E. Pallecchi, R. Ferreira, G. Fève, J.-M. Berroir, and B. Plaçais, "Supercollision cooling in undoped graphene," Nat. Phys. **9**, 109 (2013).

[14] R. Bistritzer and A. H. MacDonald, "Electronic cooling in graphene," Phys. Rev. Lett. **102**, 206410 (2009).

[15] P. Wei, W. Bao, Y. Pu, C. N. Lau, and J. Shi, "Anomalous thermoelectric transport of Dirac particles in graphene," Phys. Rev. Lett. **102**, 166808 (2009).

[16] Y. M. Zuev, W. Chang, and P. Kim, "Thermoelectric and magnetothermoelectric transport measurements of graphene," Phys. Rev. Lett. **102**, 096807 (2009).

[17] G. Skoblin, J. Sun, and A. Yurgens, "Graphene bolometer with thermoelectric readout and capacitive coupling to an antenna," Appl. Phys. Lett. **112**, 063501 (2018).

[18] J. Carr, *Microwave & Wireless Communications Technology* (Butterworth-Heinemann, 1996).

[19] G. Giovannetti, P. A. Khomyakov, G. Brocks, V. M. Karpan, J. van den Brink, and P. J. Kelly, "Doping graphene with metal contacts," Phys. Rev. Lett. **101**, 026803 (2008).

[20] T. Cusati, G. Fiori, A. Gahoi, V. Passi, M. C. Lemme, A. Fortunelli, and G. Iannaccone, "Electrical properties of graphene-metal contacts," Sci. Rep. **7**, 5109 (2017).

[21] F. A. Chaves, D. Jiménez, A. W. Cummings, and S. Roche, "Physical model of the contact resistivity of metal-graphene junctions," J. Appl. Phys. **115**, 164513 (2014).

[22] Because of the ambipolarity of the transport properties, rectification in graphene *p-n* junctions, i.e., the appearance of a dc signal stems from the thermoelectric effects.

[23] M. Hempel, A.-Y. Lu, F. Hui, T. Kpulun, M. Lanza, G. Harris, T. Palacios, and J. Kong, "Repeated roll-to-roll transfer of two-dimensional materials by electrochemical delamination," Nanoscale **10**, 5522–5531 (2018).

[24] M. Khan, K. Indykiewicz, P. L. Tam, and A. Yurgens, "High mobility graphene on EVA/PET," Nanomaterials **12**, 331 (2022).

[25] S. Ullah, X. Yang, H. Q. Ta, M. Hasan, A. Bachmatiuk, K. Tokarska, B. Trzebicka, L. Fu, and M. H. Rummeli, "Graphene transfer methods: A review," Nano Res. **14**, 3756–3772 (2021).

[26]S. D. Ganichev, E. Ziemann, T. Gleim, W. Prettl, I. N. Yassievich, V. I. Perel, I. Wilke, and E. E. Haller, "Carrier tunneling in high-frequency electric fields," Phys. Rev. Lett. **80**, 2409–2412 (1998).
[27]V. A. Shalygin, H. Diehl, C. Hoffmann, S. N. Danilov, T. Herrle, S. A. Tarasenko, D. Schuh, C. Gerl, W. Wegscheider, W. Prettl, and S. D. Ganichev, "Spin photocurrents and the circular photon drag effect in (110)-grown quantum well structures," JETP Lett. **84**, 570–576 (2007).
[28]S. D. Ganichev, P. Schneider, V. V. Bel'kov, E. L. Ivchenko, S. A. Tarasenko, W. Wegscheider, D. Weiss, D. Schuh, B. N. Murdin, P. J. Phillips, C. R. Pidgeon, D. G. Clarke, M. Merrick, P. Murzyn, E. V. Beregulin, and W. Prettl, "Spin-galvanic effect due to optical spin orientation in n-type GaAs quantum well structures," Phys. Rev. B **68**, 081302(R) (2003).
[29]S. D. Ganichev, Y. V. Terent'ev, and I. D. Yaroshetskii, "Photon-drag photodetectors for the far-IR and submillimeter regions," Sov. Tech. Phys. Lett. **11**, 20 (1985).
[30]P. H. Tan, W. P. Han, W. J. Zhao, Z. H. Wu, K. Chang, H. Wang, Y. F. Wang, N. Bonini, N. Marzari, N. Pugno, G. Savini, A. Lombardo, and A. C. Ferrari, "The shear mode of multilayer graphene," Nat. Mater. **11**, 294–300 (2012).
[31]A. C. Ferrari and D. M. Basko, "Raman spectroscopy as a versatile tool for studying the properties of graphene," Nat. Nanotechnol. **8**, 235–246 (2013).
[32]N. Sule, K. J. Willis, S. C. Hagness, and I. Knezevic, "Terahertz-frequency electronic transport in graphene," Phys. Rev. B **90**, 045431 (2014).
[33]F. Wendler, M. Mittendorff, J. C. König-Otto, S. Brem, C. Berger, W. A. de Heer, R. Böttger, H. Schneider, M. Helm, S. Winnerl, and E. Malic, "Symmetry-breaking supercollisions in Landau-quantized graphene," Phys. Rev. Lett. **119**, 067405 (2017).
[34]The sign of doping can vary depending on the metal.[19] In most cases described here, it was Au/Ti contacts, which induce *n* doping.
[35]K. J. Tielrooij, L. Piatkowski, M. Massicotte, A. Woessner, Q. Ma, Y. Lee, K. S. Myhro, C. N. Lau, P. Jarillo-Herrero, N. F. van Hulst, and F. H. L. Koppens, "Generation of photovoltage in graphene on a femtosecond timescale through efficient carrier heating," Nat. Nanotechnol. **10**, 437 (2015).
[36]A. Yurgens, "Large responsivity of graphene radiation detectors with thermoelectric readout: Results of simulations," Sensors **20**, 1930 (2020).